Central European Journal of Energetic Materials
ISSN 1733-7178; e-ISSN 2353-1843

Cent. Eur. J. Energ. Mater. 2021, *18*(1): 46-62; DOI 10.22211/cejem/134798
Article is available in PDF-format, in colour, at:
http://www.wydawnictwa.ipo.waw.pl/cejem/Vol-18-Number1-2021/CEJEM_01127.pdf

Research paper

Performance of Mn/Bi_2O_3 Pyrotechnic Time Delay Compositions

Shepherd M. Tichapondwa*, Shasha Guo, Willem E. Roux

Institute of Applied Materials, Department of Chemical Engineering, University of Pretoria, Private Bag X20, Hatfield, 0028, Pretoria, South Africa
**E-mail:* Shepherd.Tichapondwa@up.ac.za

Abstract: Chemical time delay detonators are used widely in mine blasting applications. In order to achieve effective blasting, detonations must follow a precisely controlled timing sequence in a specified firing pattern. Silicon fuel-based pyrotechnic compositions are widely used in mining detonators and are well studied. However, some of these formulations are deemed to be problematic, as they contain heavy metals which are bio-accumulative and toxic to the environment. Therefore, there is need to explore alternative formulations which are suitable for these applications. Manganese-fueled systems are attractive due to their metallic properties and several oxidation states of the manganese fuel. This study focused on characterizing the burn properties of Mn/Bi_2O_3 compositions for slow to intermediate time delay applications. The compositions supported combustion in the 25 to 55 wt.% Mn range in an inert helium atmosphere. Burn rates between 2.5 and 11.2 $mm \cdot s^{-1}$ were recorded in open burn tests, whilst closed burn tests in glass tubes resulted in burn rates of 6.3 to 11.2 $mm \cdot s^{-1}$. Both X-ray diffraction analysis of the reaction products and thermodynamic simulations confirmed that MnO and Bi are the main reaction products, with unreacted Mn and Bi_2O_3 also being detected. This suggests that the dominant reaction for this composition is a simple thermite-type reaction.

Keywords: manganese, bismuth trioxide, time delay, pyrotechnics, binder

1 Introduction

Pyrotechnic delay compositions are used extensively in both military and mining applications. Depending on the final application, there is a need to produce formulations with tunable burn rates, *e.g.* by adjusting the ratio of the constituent reagents. The delay compositions generally consist of one or more oxidizers in combination with one or more fuels [1, 2]. The selection of the oxidizer for a given fuel is dependent on the desired energy output, the reaction rate and the physical state of the reaction products. Many factors influence the burn behaviour of a composition; these must be considered when designing a delay composition [3]. Parameters such as the nature of the fuel and the oxidant, the mixture stoichiometry, the particle size distributions, the presence of additives such as binders and the quality of mixing are regarded as the most important. Numerous fuels have been used in formulating pyrotechnic delay compositions. Silicon fuelled compositions are the most widely used and studied [4]. However, silicon as a fuel creates some problems in that it is a metalloid with low thermal diffusivity and the corresponding compositions feature relatively high activation energies [3]. It is therefore of interest to explore other fuel options. Manganese has been identified as a possible candidate due to its metallic properties and the fact that it can exist in several oxidation states.

Manganese has been explored as fuel in a number of systems including:

- $Mn/BaCrO_4/PbCrO_4$, Mn/BaO_2 and Mn/SrO_2 [5],
- Mn/SbO_3 [6],
- Mn/Bi_2O_3, Mn/V_2O_5, Mn/Cu_2O [7], and
- $Sn/Mn/BiO_3$ [8].

The Mn/MnO_2 composition in particular, has received considerable attention [7, 9, 10]. These Mn-fuelled formulations have demonstrated a wide range of burn rates. Although several Mn-based formulations have been reported in the literature, most studies have focused on the measurement of burn rates with little attention being paid to characterizing other burn properties or understanding the reaction mechanisms. The present study has focused on characterizing the burn properties of Mn/Bi_2O_3 formulations. The effect of a commonly used binder on the burn properties was also investigated.

2 Materials and Methods

2.1 Materials

The manganese powder and bismuth trioxide were both supplied by Sigma Aldrich, whilst polyvinyl alcohol (PVA) with a molecular weight in the range 31000-50000 g/mol, and a 98-99% degree of hydrolysis, was obtained from Alfa Aesar. The purity and phases of these materials were analysed using X-ray diffraction (XRD). The Brunauer-Emmett-Teller (BET) surface area was measured with a Micrometrics Tristar II BET instrument and the particle size distributions were determined with a Mastersizer Hydrosizer 2000 instrument, using water as the dispersion medium.

2.2 Composition preparation

The compositions were prepared using a brush-mixing technique. The required amount of reagents needed to prepare the different compositions were first weighed out before brushing them repeatedly (*i.e.* 5 times) through a 75 µm sieve. This facilitated disintegration of any agglomerates present and ensured good mixing.

2.3 Compositions with PVA binder

A master solution of 10 wt.% PVA was prepared by dissolving the binder powder in distilled water heated to 70 °C. This solution was then used to prepare lower binder concentration solutions as required. A 40 wt.% solids slurry was prepared, with the solids ratio being maintained at a 30 wt.% Mn composition. The slurry was stirred for 2 h to allow for good mixing before being dried at 60 °C. The resultant power was ground and sieved before being tested for its burn properties.

2.4 Burn rate measurements

Open burn rate measurements were determined using an in-house test rig (Figure 1). The compositions were compacted into a 4 mm wide and 2 mm deep channel machined into a pyrophyllite block. Two thin copper wire strands were placed 40 mm apart over the compressed composition and held under tension. After ignition, the hot slag generated by the combustion wave melted and severed these wires. The first loss of continuity served as the initiating impulse for starting the stopwatch, while the second triggered the end of the burn time. The burn rate was calculated as the ratio of column length to the recorded burn time. All of the tests were repeated five times for statistical purposes.

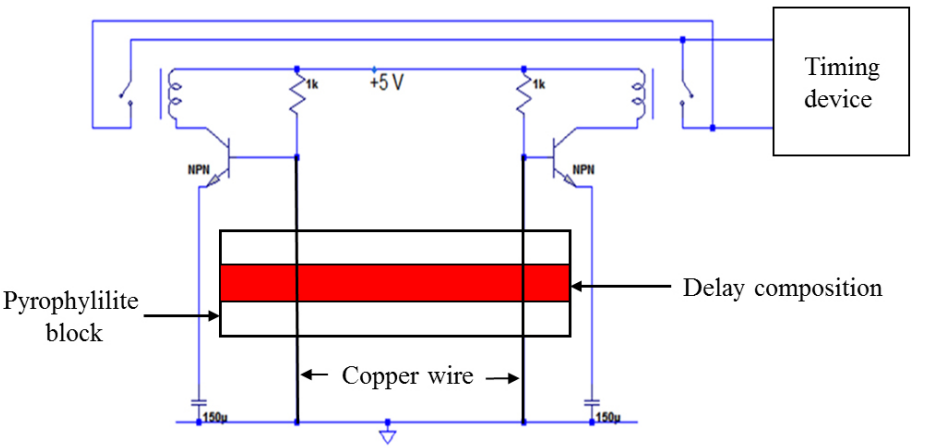

Figure 1. Burn rate measuring arrangement

Confined burn rate measurements were conducted by compressing the compositions in 50 mm borosilicate glass tubes with an internal diameter of 6 mm. The density of all samples was equal to 47 ±1% of their theoretical maximum density (TMD). Ignition was triggered with an electric fuse positioned in contact with the composition. The burn rates were then recorded using a Canon Power Shot SX260HS digital camera at a frame rate of 240 Hz.

2.5 Characterization

Differential thermal analysis (DTA) was performed on a Shimadzu DTA-50 instrument. Approximately 20 mg of sample and of a reference standard (α-Al_2O_3) were weighed into separate alumina pans. 500 µm thick copper disks were placed at the bottom of the sample pans. These acted as heat sinks to protect the DTA temperature detector from high temperature excursions [11]. DTA runs of pure manganese were carried out in both oxygen and inert argon atmospheres, whilst the mixed compositions were run in argon. The temperature was scanned from ambient temperature to 1000 °C at a scan rate of 50 °C·min^{-1} with the gas flowing at 20 mL·min^{-1}.

Enthalpy measurements were conducted on a Parr 6200 bomb calorimeter using a 1104B 240 mL high strength pressure vessel. A proprietary starter (200 mg) with known energy output initiated the samples, which weighed between 2 and 3 g [12]. The starter was ignited with an electrically heated 30-gauge Nichrome wire. The tests were conducted in an inert helium atmosphere at a pressure of 3.0 MPa. Each determination was carried out in triplicate, and the final results reported were corrected for the effect contributed by the starter used.

X-ray diffraction (XRD) analysis was performed on a Siemens D-501 automated diffractometer operated at 40 kV and 40 mA using CuKα radiation (λ = 1.5406 Å). This apparatus was equipped with a divergence slit of 1° and a receiving slit of 0.05°. The samples were scanned from between 3 to 90° on the 2θ-scale, with a counting time of 1.5 s at room temperature.

The morphology of the particles was determined using a Zeiss Ultra Plus 55 field emission scanning electron microscope (FESEM). This was fitted with an InLens detector and the acceleration voltage was set at 1 kV. The reagent powders were coated with conductive carbon using an EMITECH K950X coater.

3 Results and Discussion

3.1 Powder Characteristics

X-ray diffraction analysis confirmed that all of the raw materials were of high purity, with both the manganese and bismuth trioxide being of the α-phase (Figure 2). Table 1 gives a summary of the particle size distribution and BET surface area of the powders. Both materials had a broad particle size distribution. Figure 3 shows the morphology of the particles used to prepare the compositions. The manganese particles were predominantly of an irregular shape with sharp edges, while the Bi_2O_3 had much smaller particles with smooth surfaces. Although the d_{50} particle size for both reagents was in the micron range, the FESEM images revealed that Bi_2O_3 consisted of agglomerates made up of primary particles in the nano size-range.

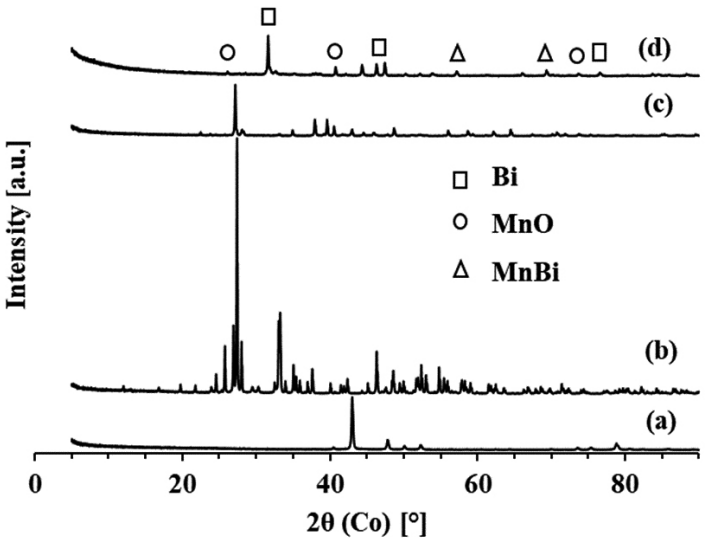

Figure 2. XRD scans of (a) pure Mn; (b) pure Bi_2O_3 powder, as well as the reaction products of (c) 40 wt.% Mn/Bi_2O_3 and (d) 45 wt.% Mn/Bi_2O_3

Table 1. Volume-based particle size distribution and BET surface areas of the raw materials used

Raw material	d_{10} [μm]	d_{50} [μm]	d_{90} [μm]	BET surface area [$m^2\ g^{-1}$]
Mn	6.5	22.2	49.4	0.34
	–[a]	6.0[a]	–[a]	0.60[a]
Bi_2O_3	1.5	3.7	10.3	0.29

[a] in Ref. [7]

3.2 Differential thermal analysis

Figure 4 shows the DTA signals obtained for pure Mn in argon and oxygen atmospheres, as well as the response signal of a 55 wt.% Mn/Bi_2O_3 composition. Pure manganese in argon resulted in two endotherms at *ca.* 780 and 960 °C, respectively. These were attributed to the first two phase transition events for manganese described in Scheme I. The transition temperatures were however somewhat different from those reported by Rapoport and Kennedy [13].

$$\alpha\text{Mn} \xrightarrow{727^\circ\text{C}} \beta\text{Mn} \xrightarrow{1094^\circ\text{C}} \gamma\text{Mn} \xrightarrow{1132^\circ\text{C}} \delta\text{Mn} \xrightarrow{1244^\circ\text{C}} \mathit{Liquid}$$

Scheme I. Phase transitions of manganese in an inert atmosphere reported by Rapoport and Kennedy [13]

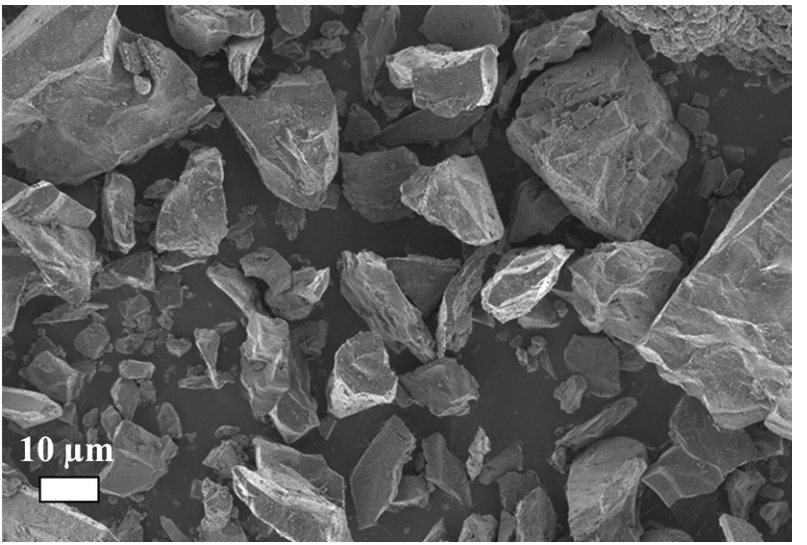

(a)

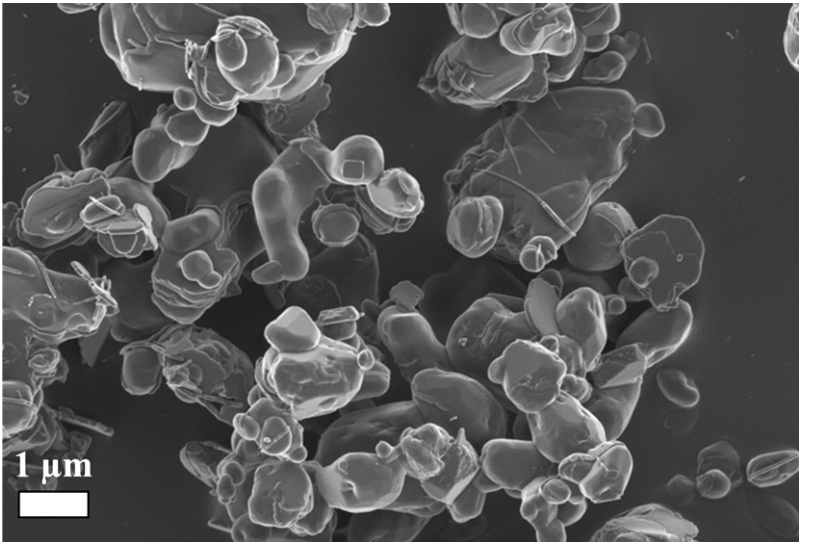

(b)

Figure 3. FESEM images of (a) manganese and (b) bismuth trioxide

The DTA response of pure manganese in an oxygen atmosphere resulted in two distinct exotherms, the first being a broad peak in a temperature range from 570 to 730 °C. This was attributed to the gradual oxidation of Mn to MnO.

The second sharp peak at *ca.* 770 °C was ascribed to the further oxidation of MnO to Mn_2O_3 [6, 7].

Due to instrument limitations, the DTA response signal for pure Bi_2O_3 was not determined. This is because upon melting, Bi_2O_3 "wets" the alumina crucibles which then fuse to the DTA sensor upon cooling. However, it is reported that Bi_2O_3 has a phase transition from the monoclinic α-phase to the cubic δ-Bi_2O_3 at 729 °C, before melting at 824 °C [14].

$$\alpha\ Bi_2O_3 \xrightarrow{729℃} \delta\ Bi_2O_3 \xrightarrow{824℃} Liquid$$

Scheme II. Phase transitions of bismuth oxide at its related temperatures [14]

The Mn/Bi_2O_3 system had an ignition temperature of *ca.* 705 °C. This suggests that ignition occurs as soon as both crystal lattices become unstable before phase transition. Tamman used the ratio of the temperature of the solid to its melting point as a rough measure of lattice loosening [15]. Ionic surface mobility was reported to become effective at a T/T_m ratio of 0.3, while lattice diffusion commences at a T/T_m ratio exceeding 0.5. The T/T_m ratios for Mn and Bi_2O_3 at the ignition temperature were 0.57 and 0.86, respectively. This suggests that lattice diffusion is the dominant lattice loosening mechanism in Mn. The markedly higher ratio for Bi_2O_3 can be attributed to the 'Hedvall effect', which states that enhanced reactivity occurs near other phase transition temperatures [1, 15].

The DTA signal for the composition treated with the PVA binder (Figure 4, curve (d)) showed a significant decrease in the ignition temperature. The signal featured an initial small broad exotherm at 590 °C followed by a sharp exotherm at *ca.* 670 °C. This suggested that the PVA binder sensitizes the composition by participating in the reaction. It is worth noting that the DTA signal of the pyrotechnic composition coincided with the broad Mn to MnO oxidation peak reported for manganese in an oxygen atmosphere. It was therefore postulated that once the crystal lattices of the reactants become unstable, the driving redox reaction is similar to Scheme III.

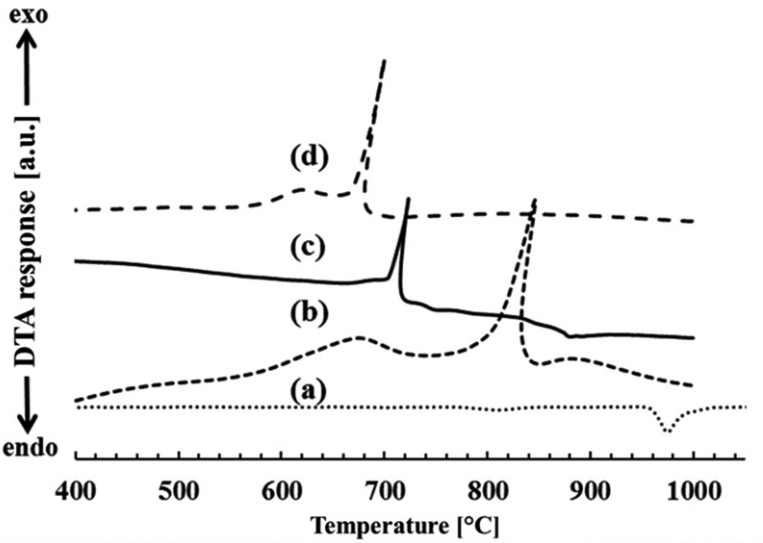

Figure 4. DTA response signals of (a) Mn in inert argon atmosphere; (b) Mn in oxygen atmosphere; (c) 55 wt.% Mn/Bi_2O_3 composition in argon atmosphere; (d) 30 wt.% Mn/Bi_2O_3 composition treated with 3 wt.% PVA binder in argon atmosphere

$$3Mn + Bi_2O_3 \rightarrow 2Bi + 3MnO$$

Scheme III. Stoichiometric redox reaction of Mn with Bi_2O_3

Figure 5 reveals that the ignition temperature of the various compositions remains relatively constant regardless of the variation in fuel content. Although the ignition temperature did not change, there was a progressive shift in the shape of the curves with increase in fuel composition. The change in the shape of the DTA response curves was indicative of a decrease in energy output with the increase in fuel content. Bomb calorimetric measurements (Table 2) confirmed this postulation as the energy output decreased from 1.15 $kJ \cdot g^{-1}$ at 30 wt.% Mn to 0.53 $kJ \cdot g^{-1}$ at 55 wt.% Mn.

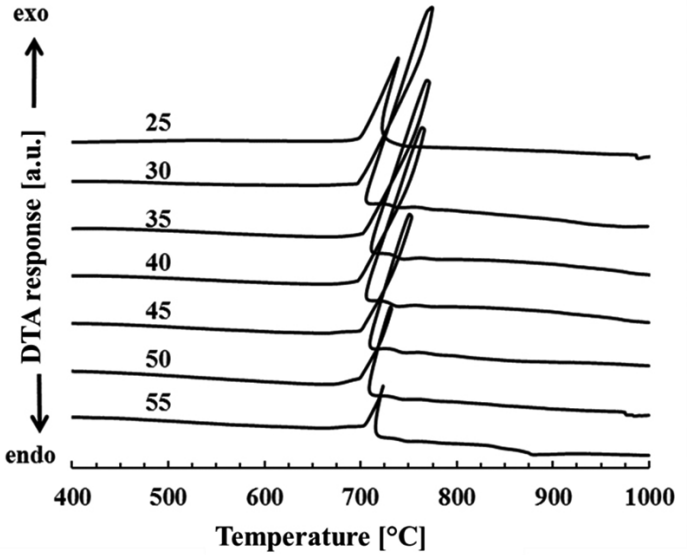

Figure 5. DTA response of different compositions of Mn/Bi_2O_3 in argon atmosphere

Table 2. Summary of the burn properties of the Mn/Bi_2O_3 pyrotechnic compositions

Mn content [wt.%]	Burning rate[a]		Energy output (bomb calorimetry) [kJ·g^{-1}]	Ignition temperature (DTA) [°C]	Adiabatic reaction temperature (EKVI simulation) [°C]
	open air [mm·s^{-1}]	glass tube [mm·s^{-1}]			
25	9.3 ±1.6	8.0 ±0.4	0.95	697.5	1565
30	11.2 ±1.7	11.2 ±0.8	1.04	702.2	1559
35	8.9 ±1.2	8.9 ±1.2	1.15	701.8	1559
40	8.1 ±1.2	6.3 ±1.8	0.92	704.6	1559
45	6.6 ±0.6	–	0.82	702.3	1456
50	3.5 ±0.1	–	0.61	705.2	1352
55	2.5 ±0.2	–	0.53	707.7	1242

[a] The burning rates of open air and glass tube combustions were obtained from delay compositions packed into pyrophyllite open-air channels and glass tubes, respectively.

3.3 EKVI simulations and XRD results

Thermodynamic simulations were performed using EKVI software with the aim of determining the effect of the fuel to oxidizer ratio on the product distribution and the adiabatic reaction temperature. The equilibrium compositions

were computed based on the assignment of reaction criteria, which included specifying the reactant ratios, pressure (or volume), temperature and possible products [16]. Figure 6 summarises the simulated reaction products obtained at the corresponding adiabatic reaction temperatures. The system reached a maximum reaction temperature of 1565.8 °C at ≈26 wt.% Mn. This is in agreement with the predicted stoichiometry from the thermite-type reaction shown in Scheme III. The maximum fractions of MnO and Bi are formed at this composition. Fuel rich compositions above 40 wt.% Mn were predicted to form an intermetallic MnBi compound. The formation of this intermetallic compound is consistent with a combination of the standard thermite reaction and an additional exothermic intermetallic reaction represented in Scheme IV. The A similar sequence of reactions has been reported for the Mn/Sb_2O_3 composition [6]. It is worth noting that the EKVI simulations for this system were similar to the behaviour simulated using FactSage [17].

$$5Mn + Bi_2O_3 \rightarrow 3MnO + 2MnBi$$

Scheme IV. Balanced reaction for the fuel rich combination of Mn and Bi_2O_3 to form an intermetallic compound

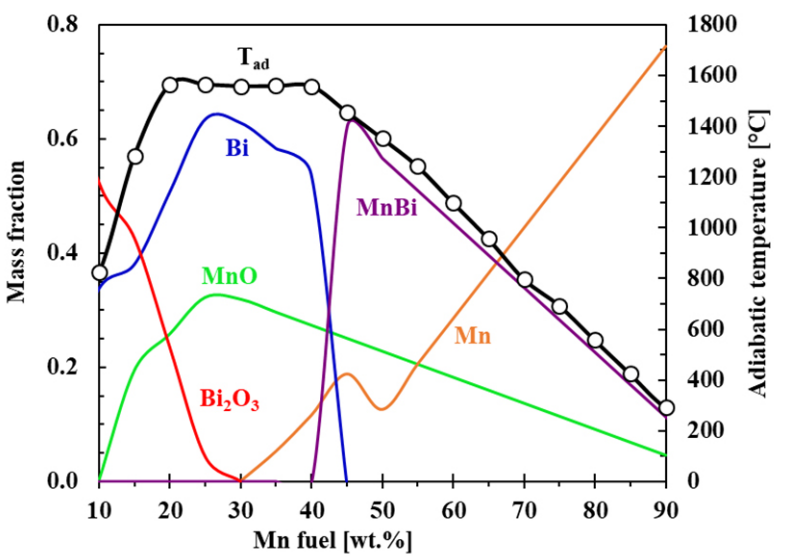

Figure 6. Adiabatic flame temperature and total product formation resulting from EKVI thermodynamic simulations for the reaction of Mn with Bi_2O_3

Figure 7 presents the EKVI simulation of a 30 wt.% Mn composition in the presence of varying amounts of PVA binder. Based on the product distribution, it is clear that the PVA participates in the reaction as it reduces the adiabatic temperature and hence alters the products formed. Three main reaction regions were postulated based on the product distribution from the simulations, as shown in Scheme V.

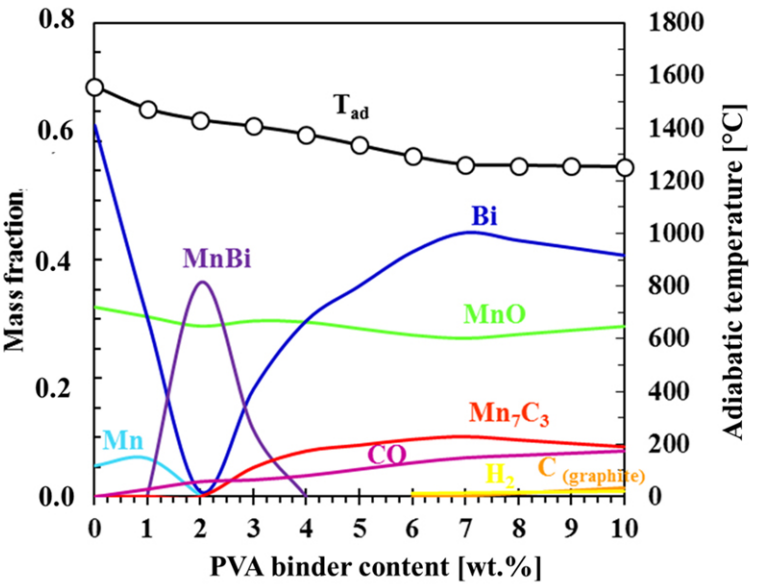

Figure 7. Adiabatic flame temperature and total product formation resulting from EKVI thermodynamic simulations for a 30:70 (by mass) Mn/Bi_2O_3 composition in the presence of varying amounts of PVA binder

$$2Mn + Bi_2O_3 + C_2H_4O \rightarrow 2MnO + 2Bi + 2H_2 + 2CO \quad (a)$$
$$4Mn + Bi_2O_3 + C_2H_4O \rightarrow 2MnO + 2MnBi + 2H_2 + 2CO \quad (b)$$
$$10Mn + Bi_2O_3 + 5C_2H_4O \rightarrow 3MnO + 2Bi + Mn_7C_3 + 10H_2 + 5CO + 2C \quad (c)$$

Scheme V. Main stoichiometric reactions of the Mn/Bi_2O_3 composition in the presence of PVA with the following binder contents (a) < 1 wt.% PVA; (b) 2 wt.% PVA; (c) > 4 wt.% PVA

A representative XRD spectrum for the reaction products is shown in Figure 2. XRD analysis of the reaction products from the different compositions revealed the presence of MnO and Bi as the main reaction products. Unreacted Mn

and Bi_2O_3 were also detected. It is worth noting that no intermetallic MnBi was detected for the 40 wt.% composition, however the 45% composition showed the presence of MnBi in the residue (Figure 2). These observations agree with the product distributions predicted by the EKVI software where MnBi is only present above 40 wt.% Mn. These results confirm the hypothesis that the dominant reaction proceeds *via* the pure thermite-type redox reaction shown in Scheme III for compositions with a fuel content below 40 wt.% Mn. At higher fuel contents, the reactions presented in Scheme V become more pronounced.

3.4 Burn rate measurements

Open burn combustion was sustained in compositions which contained 25 to 55 wt.% Mn, with the fastest burn rate being 11.2 $mm \cdot s^{-1}$ recorded for the 30 wt.% Mn composition (Figure 8). The burn rate decreased with increasing fuel content. The 55 wt.% Mn composition had the slowest burn rate of 2.5 $mm \cdot s^{-1}$. Similar burn rates were also obtained for compositions packed in glass tubes. This was despite a difference in the packed densities of the two configurations, where the average density of the pyrotechnic composition was 3.88 ±0.08 $g \cdot cm^{-3}$ compared to its density in the open air pyrophyllite channel, which was 2.80 ±0.2 $g \cdot cm^{-3}$. However, complete combustion was only sustained in a narrower fuel range (25 to 40 wt.% Mn) for the glass tubes. It is postulated that the presence of atmospheric oxygen in the open burn tests could have aided in extending the burn range. The trend observed in this study was the complete opposite to the results presented by Swanepoel *et al.* [7] who found an increase in burn rate with increasing fuel content. They reported a maximum burn rate of *ca.* 21 $mm \cdot s^{-1}$ for the 60 wt.% Mn composition. They however confined their compositions into aluminium delay elements, which have a higher thermal conductivity compared to the clay-based pyrophyllite block and glass tubes used in the present study. Although the study by Swanepoel *et al.* [7] reported that a compression pressure above 105 MPa resulted in "dead pressed" compositions, an indication of the TMD or actual density was not given. Their observations however suggest that the confinement density influences the burn properties of this composition. It should also be noted that the d_{50} particle size of the Mn used in the present study was *ca.* 4 times larger than the one used by Swanepoel *et al.* [7]. Particle size is known to significantly influence the burn rate of pyrotechnic compositions [6, 18], it is therefore possible that this could have also contributed to the differences in the burn trends observed in Figure 8. Lastly, closed systems provided by the delay elements would also be influenced by the convective heating effects presented by any gaseous phases formed. This allows for preheating of the pre-ignition zones adjacent to the combustion zone, ultimately increasing the reaction rate [15].

The Mn/Bi_2O_3 composition was very sensitive to the presence of PVA binder (Figure 9). Addition of as little as 0.5 wt.% binder decreased the burn rate from 11.2 to 5.6 $mm \cdot s^{-1}$. A 90% burn rate decrease was observed when 3 wt.% PVA was added, and any further binder addition resulted in incomplete propagation or failed ignition. This observation is thought to result from energy being drawn away from the main reaction towards the degradation of the organic binder. This reduces the amount that is transferred to the pre-reaction zone, which in turn limits the reactivity of the composition.

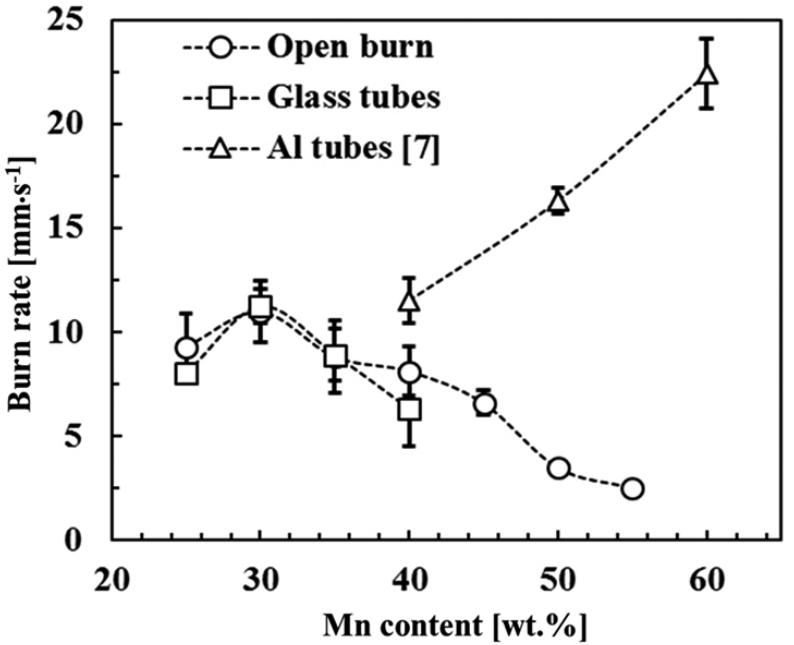

Figure 8 Effect of fuel content on the burn rate of the Mn/Bi_2O_3 composition under open burn, glass tube and full detonator [7] conditions

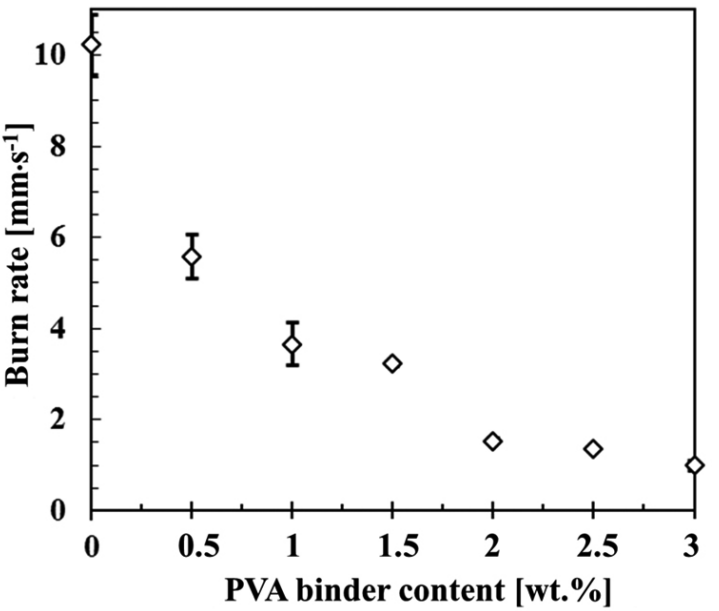

Figure 9. Effect of PVA binder content on the burn rate of a 35 wt.% Mn/Bi_2O_3 composition

4 Conclusions

- The Mn/Bi_2O_3 pyrotechnic time delay composition was characterised and its basic reaction mechanism was established.
- The ignition temperature was determined to be significantly lower than the melting points of both reactants. This was attributed to the destabilization of the crystal structures of both reactants as they near phase transitions.
- The burn rate and energy output decreased with increasing fuel loading, with a maximum burn rate of 11.3 $mm \cdot s^{-1}$ recorded for 35 wt.% Mn.
- XRD and EKVI simulations revealed MnO and Bi as the main reaction products, which suggests that a simple thermite-type redox reaction is the dominant reaction.
- The presence of PVA binder had a negative effect on the burn properties of the composition as well as the predicted product distribution.

References

[1] McLain, J.H. *Pyrotechnics: From the Viewpoint of Solid State Chemistry*. Franklin Institute Press, Philadelphia, **1980**.

[2] Berger, B. Parameters Influencing the Pyrotechnic Reaction. *Propellants Explos. Pyrotech*. **2005**, *30*(1): 27-35.

[3] Kosanke, K.; Kosanke, B.; Sturman, B.; Shimizu, T.; Wilson, M.; von Maltitz, I.; Hancox, R.; Kubota, N.; Jennings-White, C.; Chapman, D. *Pyrotechnic Chemistry.* Pyrotechnic Reference Series, No. 4. Huntingdon, UK, Journal of Pyrotechnics Inc. & CarnDu Ltd, **2000**.

[4] Koch, E.C.; Clement, D. Special Materials in Pyrotechnics: VI. Silicon – an Old Fuel with New Perspectives. *Propellants Explos. Pyrotech*. **2007**, *32*(3): 205-212.

[5] Drennan, R.L.; Brown, M.E. Binary and Ternary Pyrotechnic Systems of Mn and/or Mo and BaO_2 and/or SrO_2. Part 2. Combustion Studies. *Thermochim. Acta* **1992**, *208*: 223-246.

[6] Montgomery, Y.C.; Focke, W.W.; Atanasova, M.; Del Fabbro, O.; Kelly, C. Mn+Sb_2O_3 Thermite/Intermetallic Delay Compositions. *Propellants Explos. Pyrotech*. **2016**, *41*(5): 919-925.

[7] Swanepoel, D.; Del Fabbro, O.; Focke, W.W.; Conradie, C. Manganese as Fuel in Slow-burning Pyrotechnic Time Delay Compositions. *Propellants Explos. Pyrotech*. **2010**, *35*(2): 105-113.

[8] Guo, S.; Focke, W.W.; Tichapondwa, S.M. Sn/Mn/Bi_2O_3 Ternary Pyrotechnic Time Delay Compositions. *ACS Sustain. Chem. Eng*. **2020**, *8*(38): 14524-14530.

[9] Kappagantula, K.S.; Clark, B.; Pantoya, M.L. Flame Propagation Experiments of non-Gas-Generating Nanocomposite Reactive Materials. *Energy Fuels* **2011**, *25*: 640-646.

[10] Miklaszewski, E.J.; Shaw, A.P.; Poret, J.C.; Son, S.F.; Groven, L. Performance and Aging of Mn/MnO_2 an Environmentally Friendly Energetic Time Delay Composition. *ACS Sustain. Chem. Eng*. **2014**, *2*: 1312-1317.

[11] Ilunga, K.; Del Fabbro, O.; Yapi, L.; Focke W.W. The effect of Si-Bi_2O_3 on the Ignition of the Al-CuO Thermite. *Powder Technol*. **2011**, *205*: 97-102.

[12] Tichapondwa, S.M.; Focke, W.W.; Del Fabbro, O.; Gisby, J.; Kelly, C. A Comparative Study of Si-$BaSO_4$ and Si-$CaSO_4$ Pyrotechnic Time-delay Compositions. *J. Energ. Mater.* **2016**, *34*: 342-356.

[13] Rapoport, E.; Kennedy, G.C. Phase Diagram of Manganese to 40 kbars. *J. Phys. Chem. Solids*. **1966**, 27: 93-98.

[14] Wells, A. *Structural Inorganic Chemistry*. Oxford University Press, **2012**.

[15] Focke, W.W.; Tichapondwa, S.M.; Montgomery, Y.C.; Grobler, M.; Kalombo, L. Review of Gasless Pyrotechnic Time Delays. *Propellants Explos. Pyrotech.* **2019**, *44*(1): 55-93.

[16] Govender, D.; Focke, W.W.; Tichapondwa, S.M.; Cloete, W.E. Burn Rate of Calcium Sulfate Dehydrate – Aluminium Thermites. *ACS Appl. Mater. Interfaces*. **2018**, *10*(24): 20679-20687.

[17] Shaw, A.P.G. *Thermitic Thermodynamics: A Computational Survey and Comprehensive Interpretation of over 800 Combinations of Metals, Metalloids, and Oxides.* CRC Press, **2020**.
[18] Tichapondwa, S.M.; Focke, W.W.; Del Fabbro, O.; Labuschagne, G. The Effect of Additives on the Burning Rate of Silicon-Calcium Sulfate Pyrotechnic Delay Compositions. *Propellants Explos. Pyrotech.* **2016***, 41*(4): 732-739.

Received: March 7, 2020
Revised: March 23, 2021
First published online: March 30, 2021